



Connecting particle interactions to agglomerate morphology and rheology of boehmite nanocrystal suspensions



J.S. Weston^{a,*}, J. Chun^{b,c,*}, G. Schenter^b, K. Weigandt^d, M. Zong^b, X. Zhang^b, K.M. Rosso^b, L.M. Anovitz^{e,*}

^aRussell School of Chemical Engineering, University of Tulsa, Tulsa, OK 74104, United States

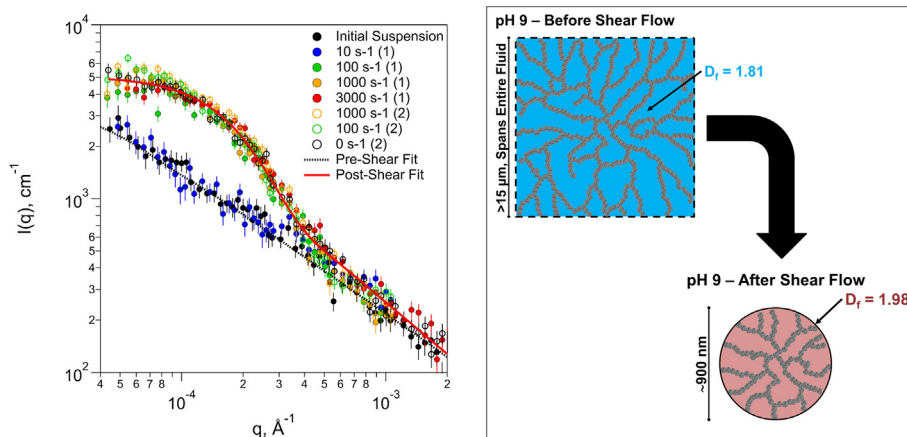
^bPacific Northwest National Laboratory, Richland, WA 99354, United States

^cBenjamin Levich Institute, CUNY City College of New York, New York, NY 10031, United States

^dNIST Center for Neutron Research, National Institute of Standards and Technology, Gaithersburg, MD 20899, United States

^eOak Ridge National Laboratory, Oak Ridge, TN 37830, United States

GRAPHICAL ABSTRACT



ARTICLE INFO

Article history:

Received 16 October 2019

Revised 27 March 2020

Accepted 28 March 2020

Available online 31 March 2020

Keywords:

Particles

Suspensions

Rheology

Neutron scattering

Boehmite

ABSTRACT

Hypothesis: The rheology of complex suspensions, such as nuclear waste slurries at the Hanford and Savannah River sites, imposes significant challenges on industrial-scale processing. Investigating the rheology and connecting it to the agglomerate morphology and underlying particle interactions in slurries will provide important fundamental knowledge, as well as prescriptive data for practical applications. Here, we use suspensions of nano-scale aluminum oxyhydroxide minerals in the form of boehmite as an analog of the radioactive waste slurry to investigate the correlation between particle interactions, agglomerate morphology, and slurry rheology.

Experiments: A combination of Couette rheometry and small-angle scattering techniques (independently and simultaneously) were used to understand how agglomerate structure of slurry changes under flow and how these structural changes manifest themselves in the bulk rheology of the suspensions.

Findings: Our experiments show that the boehmite slurries are thixotropic, with the rheology and structure of the suspensions changing with increasing exposure to flow. In the slurries, particle agglomerates begin as loose, system-spanning clusters, but exposure to moderate shear rates causes the agglomerates to irreversibly consolidate into denser clusters of finite size. The structural changes directly influence the rheological properties of the slurries such as viscosity and viscoelasticity. Our study shows that solution

* Corresponding authors at: The University of Tulsa, Tulsa, OK, 74104, United States (J. Weston); Pacific Northwest National Laboratory, Richland, WA 99354, United States (J. Chun).

pH affects the amount of structural rearrangement and the kinetics of the rearrangement process, with an increase in pH leading to faster and more dramatic changes in bulk rheology, which can be understood via correlations between particle interactions and the strength of particle network. Nearly identical structural changes were also observed in Poiseuille flow geometries, implying that the observed changes are relevant in pipe flow as well.

© 2020 Elsevier Inc. All rights reserved.

1. Introduction

The ability to effectively and efficiently transport slurries and sludges is a key processing aspect in a wide array of industrial applications such as cosmetics, paints, health care products, concrete production, mining, and many others [1–4]. However, transport of suspensions of solid particles is particularly challenging due to complicating phenomena such as sedimentation [5–8] and particle network formation [9–14], which are strongly correlated to physicochemical conditions. For example, radioactive waste slurries located at Hanford, WA are a particularly complex class of suspensions due to high concentrations of electrolytes, caustic conditions (pHs ranging from 11 to 12), a collection of mineral solid particles and long-term irradiation of the whole. The most prevalent mineral species in the slurries are gibbsite ($\text{Al}(\text{OH})_3$) and boehmite ($\gamma\text{-AlO}(\text{OH})$) with irregular shapes and broad size distributions (from 10's of nm up to 100's of μm). The US Department of Energy (DOE) projects that it will require 50+ years and hundreds of billions of dollars to retrieve and process these materials; one of the key difficulties would be anticipating slurry rheology within and between waste holding tanks [15]. More specifically, the irregular shapes and rough surfaces of the solid particles in the waste slurries, combined with the unique physicochemical conditions, currently prohibit calculation of particle interactions. This lack of fundamental understanding poses significant challenges for describing the colloidal and hydrodynamic interactions, particle size evolution, and development of hierarchical structures in the slurries.

In most suspensions micro-scale interparticle forces control the macro-scale rheological properties of the slurry and generate mechanical resistance to an external flow field such as shearing; these interparticle forces are thus a critical component in understanding slurry rheology. They result in the generation of fluid-spanning floc structures due to aggregation, fusion, and/or coarsening [16–20] that are directly responsible for overall rheological behavior [21,22]. For example, the yield stress of attractive particle suspensions [23] is dependent on the spatial configuration of particles in agglomerates (i.e., fractal dimension of the particle network) and strength [24] of interparticle interactions. This structural effect can be just as important in determining the yield stress as the solid particle volume fraction [7]. Therefore, characterizing the correlations between the suspension rheology, physicochemical parameters (e.g., pH and salt concentrations), and the agglomerate morphology of the particle network will provide critical insights into how slurries can be processed.

Previous studies on the attractive and repulsive particle interactions of boehmite nanocrystals using dynamic light scattering (DLS) and small-angle neutron scattering (SANS) showed orientation-dependent colloidal and hydrodynamic interactions, along with the effects of ionic strength, salt species, and pH, and their influences on aggregation kinetics and agglomerate morphology in the absence of an external flow field [25,26]. In order to understand the correlation between micro-scale interparticle forces and macro-scale rheology on the basis of such previous studies, we here study changes in boehmite agglomerates structures under shear (Couette) flows and analyzed how these

structural changes manifest themselves in bulk suspension rheology. For simplicity, we have used a model dispersion containing only boehmite nanocrystals. This work focused on investigating slurries at two different pH conditions (pH 9 and pH 13) and understanding how the agglomerate morphology and rheology of the slurry changes under different flow conditions. In the first section, the slurries were subjected to a series of increasing shear rates while tracking the rheological changes. The second section investigated the time-dependence of the viscoelastic behavior and agglomerate morphology of the slurries when exposed to a single shear rate. Lastly, a brief set of experiments was used to show that similar changes to those observed in Couette flow are seen when the slurry is exposed to pressure-driven pipe (i.e., Poiseuille) flow, as well. Simple physical interpretations of our experiments, connecting to particle interactions and agglomerate morphology, will be provided.

2. Materials and methods

2.1. Preparation of boehmite nanocrystals

Boehmite nanocrystals were synthesized using our previously reported method [27]. Aluminum nitrate ($\text{Al}(\text{NO}_3)_3 \cdot 9\text{H}_2\text{O}$, $\geq 98\%$, Sigma-Aldrich Chemical Reagent Co. Ltd., USA) and sodium hydroxide (NaOH , $\geq 98\%$, Sigma-Aldrich Chemical Reagent Co. Ltd., USA) were dissolved into deionized water to make 0.25 M and 3 M solutions, respectively. Then 3 M NaOH was added into the 0.25 M $\text{Al}(\text{NO}_3)_3$ while stirring at room temperature to adjust the solution pH to ~ 10.0 . After continuous stirring for 1 h, the $\text{Al}(\text{OH})_3$ precipitates were collected by centrifugation and then washed with deionized water three times to remove all soluble salts. $\text{Al}(\text{OH})_3$ precipitates were then dispersed into deionized water and 3 M NaOH (aq.) was added. In the mixture, the concentrations of the $\text{Al}(\text{OH})_3$ precipitates [defined as the concentration of $\text{Al}(\text{III})$] and NaOH were 0.5 M and 0.2 M, respectively. 1.6 L of the mixture then was transferred into a 2 L Parr steel vessel and stirred at 100 rpm at 120 °C for 48 h. The resulting solids were recovered by centrifugation, followed by washing with deionized water three times and drying at 80 °C overnight. The sample was characterized by XRD, scanning electron microscopy (SEM), and transmission electron microscopy (TEM).

2.2. Fluid preparation

Fluids were prepared in a glovebox under an inert N_2 or Ar atmosphere to minimize exposure to air and possible formation of Na_2CO_3 . An aqueous solution at pH 14 was prepared using 18 $\text{M}\Omega\text{-cm}$ water (Milli-Q Advantage A10) sparged water and NaOH ($\geq 98\%$, Sigma-Aldrich). This solution was then diluted to the desired pH. After 24 h of equilibration, additional NaOH was added to return the samples to the desired pH values if needed. All pH values were determined using either an Orion Products glass electrode with a Denver Instruments model 250 m pH meter or a Cole-Parmer double-junction electrode with an Oakton Ion 700 pH meter.

2.3. Suspension preparation

Boehmite crystal suspensions were prepared by weighing out the desired mass of boehmite powder (i.e., 5 wt%) using a microbalance and then adding the required volume of the previously described aqueous solutions to achieve the desired mass fraction of boehmite. The listed bulk density of boehmite in the literature is 3.040 g/cm^3 , which would imply a volume fraction of ~ 0.017 for the samples measured in this work. Assuming that nanoparticles have a density equal to that of the bulk is, however, often inaccurate and this value is only a rough approximation. After weighing, unless otherwise stated, the boehmite was dispersed via sonication with a probe sonicator (500 W, 1/4" diameter tip, 70% amplitude, 5 mins at 50% duty cycle). Prior to the experiments samples were stored under inert gases in septa-sealed bottles. Samples were transferred to rheometer geometries and SANS cells under inert atmosphere when possible, or using methods to minimize exposure to air where inert gases were not available.

2.4. Rheological characterization and shear flow

Rheological measurements were conducted using an Anton Paar MCR 301 stress-controlled rheometer. Two measurement geometries were used. For offline characterization of suspension rheology a stainless steel Mooney-Ewart concentric cylinder was employed, with an inner cylinder radius of 10.5 mm and a gap between the inner and outer cylinders of 0.9 mm. A Mooney-Ewart geometry was used to ensure that the entire sample experienced a uniform shear rate. For measurements with concurrent neutron scattering a specialized RheoSANS geometry was employed consisting of a quartz Mooney-Ewart concentric cylinder with an inner cylinder radius of 24 mm and a gap between the inner and outer cylinders of 1 mm. Quartz was used in order to maximize neutron transparency and minimize parasitic neutron scattering. Both geometries were used as specified by the manufacturer and appropriate steps were taken to minimize measurement artifacts and correct for system inertia.

Poiseuille flow experiments were carried out using PEEK capillary tubing with an inside diameter of 0.8 mm. Flow was produced using New Era NE-1000 syringe pumps. The flow rate was selected to yield a wall shear rate similar to that in the Couette RheoSANS geometry. In pressure-driven flow, however, there is a gradient of shear rates across the tubing diameter. Thus, the entire sample is not subjected to an equal shear flow during a single pass through the tubing. Therefore, a short length (approx. 8 cm) of tubing was used and the sample was passed back and forth between two opposing syringe pumps a sufficient number of times to expect that the entire sample experienced some shear flow at, or near the maximum rate near the wall. As the Reynolds number inside the capillary (assuming the worst-case scenario of water viscosity) is ~ 62 , flow should be laminar. The entrance length is on the order of 3–6% of the total tubing length, and thus entrance effects should have little effect on the result. However, neither of these values account for the non-Newtonian, nor thixotropic nature of the suspension. They are meant to show that flow can be expected to be laminar and fully-developed for much of the tubing length. The number of passes through the tubing was scaled so that the 'average' sample volume experienced the wall shear rate for an amount of time roughly equivalent to that of the sample in the Couette cell (which has an almost entirely uniform shear rate throughout). While the two flow geometries are clearly not exactly physically equivalent, attempts were made to make them as similar as possible. Samples were removed from syringe pumps after 8 and 20 passes and placed in static, titanium scattering cells for USANS characterization.

2.5. Boehmite characterization

2.5.1. X-ray diffraction (XRD)

XRD measurements were performed on a Philips X'pert Multi-Purpose Diffractometer (MPD) (PANalytical, Almelo, The Netherlands) equipped with a fixed Cu anode operating at 50 kV and 40 mA. The XRD pattern was collected from 5 to $80^\circ 2\theta$. Phase identification was performed using JADE 9.5.1 from Materials Data Inc., and the 2012 PDF4 + database from the International Center for Diffraction Data (ICDD) database.

2.5.2. Transmission electron microscopy (TEM)

TEM was performed on a FEI Titan TEM (FEI, Hillsboro, OR). Samples were prepared by placing a drop of boehmite suspension ($0.2 \text{ mg}\cdot\text{mL}^{-1}$) onto a copper grid (Lacey Carbon, 300 mesh, Copper grid, Ted Pella, Inc.) and then drying under ambient conditions. The sample was imaged using an acceleration voltage of 300 kV.

2.6. Ultra-small angle neutron scattering (USANS)

All USANS measurements were made using the BT-5 Perfect Crystal Diffractometer at the NIST Center for Neutron Research (NCNR). The operating principles of this instrument and the USANS technique are described in detail by Barker et al. [28] USANS measurements were used to probe the agglomerate size and fractal dimension [29] of the gel network over a range of scattering vectors (q) from $3.9 \cdot 10^{-5} \text{ \AA}^{-1}$ to $1.2 \cdot 10^{-3} \text{ \AA}^{-1}$, corresponding to length scales ranging from $\sim 500 \text{ nm}$ to $\sim 15 \text{ }\mu\text{m}$. For static USANS measurements, samples were loaded into sealed, titanium cells with a path length ranging from 1 mm to 4 mm. Simultaneous rheology and USANS measurements were conducted using the previously described RheoSANS device. The USANS used a 5/8" circular aperture at the beam outlet, but a smaller, rectangular aperture of $18 \text{ mm} \times 10 \text{ mm}$ at the rheometer to avoid curvature effects related to the Couette cell. Data were corrected for empty-beam and background scattering, and reduced onto an absolute scale by normalizing it with the direct beam intensity in accordance to NIST reduction protocols [30]. Scattering results were analyzed and fit using the unified radius of gyration model proposed by Beaucage [31] using the SasView software package (version 4.1.0). To avoid the risks of over-fitting and over-interpreting the scattering results, a single model level with a single radius of gyration was used. This model is able to reasonably approximate the scattering from many different types of particles and particle networks; working best for mass fractal systems characterized by fractal exponents between $5/3$ and 3 . Hammouda [32] has pointed out a deficiency in the way this model handles the transitioning between the Guinier and Porod regimes, which can create fitting artifacts that appear as kinks in the fitted function. These have been sufficiently accounted for in the present work. The model allows us to obtain an agglomerate "size" and a fractal dimension of the boehmite particle network within the agglomerate. The DREAM fitting optimizer was used to fit the data in all cases, as it provides a more robust analysis of parameter uncertainty. The slit smearing of the USANS instrument was accounted for by applying a smeared resolution function to the model using SasView. A complete discussion of the DREAM algorithm and smearing functions can be found in the online SasView documentation (found at <http://www.sasview.org/docs/user/user.html>). Smearing the model (rather than desmearing the measured scattering data) minimizes mathematical artifacts and noise amplification that occurs during the desmearing process. *All of the scattering data shown in this work are the raw, slit-smeared data obtained from the USANS instrument.*

3. Results and discussion

3.1. Characterization of the boehmite nanocrystals

Given the expectation that at least some aspects of the rheological properties of the slurry derive from the properties of individual boehmite particles [27], we here summarize particle phase purity, crystallinity, and morphology. XRD patterns of the synthetic boehmite (Fig. 1a) matched well with the PDF file of pure boehmite (ICDD PDF # 00-74-1895) [25]. The strong diffraction peak located at $14.5^\circ 2\theta$ was readily assignable to (0 2 0) diffraction. The boehmite material was both phase pure at XRD detection limits, and highly crystalline. High resolution TEM images (Fig. 1b) showed that the boehmite nanocrystals are uniformly rhombic shaped nanoplatelets, with an average size (along the [1 0 1] direction) and thickness (along the [0 1 0] direction) of $19.4 (\pm 7.6)$ and $5.3 (\pm 1.4)$ nm, respectively. This suggests the boehmite particles conform to its typical morphology that presents the (0 1 0) basal surface as the dominant fraction of the geometric surface area.

3.2. Effect of increasing shear rate on boehmite nanocrystal slurries

The structural and rheological evolution of suspensions containing 5% (w/v) boehmite at pH 9 and pH 13 were studied in detail. These pH conditions were chosen to represent the range of pH commonly encountered in the relevant radioactive waste slurries. In order to probe the extent to which the agglomerate morphology and bulk suspensions viscosity are dependent on the shear history of the sample RheoUSANS measurements were conducted at a range of shear rates. The results of these tests are shown in Fig. 2, where (a) shows the USANS curves of the pH 9 sample, (b) shows the USANS curves of the pH 13 sample, and (c) shows a plot of the apparent viscosity at the start of each USANS measurement as a function of shear rate. The samples were sheared continuously at a given shear rate throughout the USANS measurements to track any hysteresis.

Prior to shearing, the scattering intensity follows a single power-law slope throughout the entire q range (black triangles in Fig. 2a). This is indicative of a fractal network of boehmite particles that either consists of agglomerates $> 16 \mu\text{m}$ in diameter or a network that uniformly spans the entire suspension. Fractal networks similar to this are observed in a wide variety of attractive particle gels, many of which demonstrate similar rheological behavior to these suspensions [33–39]. The initial structure of the particle networks, however, does vary slightly between the two pH conditions. Fitting both samples with the Beaucage model

(dashed black line in Fig. 2(a) and (b)) indicates that the fractal dimension of the network is slightly higher at pH = 13 ($D_f = 1.98 \pm 0.02$) than at pH = 9 ($D_f = 1.81 \pm 0.04$), indicating a denser the agglomerate network at pH = 13. In both cases the fitted radius of gyration is much larger than the size scales probed by USANS, indicating that the fractal clusters span the entire system. In both cases the fitted fractal dimensions are indicative of a mixture of diffusion-limited and reaction-limited aggregation [40,41]. However, further interpretation requires consideration of the particle shape of the boehmite crystals, which are non-spherical and sharp-edged. Our previous study [26], using an order of magnitude smaller particle concentration ($< 0.1 \text{ wt}\%$) clearly showed reaction-limited aggregation at pH = 9 and no salt with identical boehmite crystals, whereas at pH = 12–13 with no salt the study demonstrated a case close to diffusion-limited aggregation. However, *a priori* diffusion-limited aggregation would be more expected pH = 9 than pH = 13, as a negligible repulsive electrostatic interaction between boehmite crystals is expected near the point of zero charge (pH = 8–9). [42] This, therefore, indicates (i) the existence of significant orientation-dependent hydrodynamic and van der Waals interactions and (ii) the mitigation of the orientational dependence via a noticeable electrostatic interaction. Furthermore, the fractal dimensions (2.30 ± 0.18 from a direct measurement using a cryo-TEM and image analysis) are greater than values typically reported for spherical nanoparticles (1.5–1.9 range) for diffusion-limited cases [26]. Comparison with the key findings in the previous study suggests that (i) there must be a certain “threshold” particle concentration at which diffusion-limited aggregation begins to dominate reaction-limited aggregation, possibly with the aggregation becoming ‘arrested’ by the presence of the particle network at higher solid volume fractions (at pH = 9), and (ii) higher particle concentrations generate sparser agglomerate structures while maintaining diffusion-limited aggregation (at pH = 13). The difference in fractal dimension between pH = 13 and pH = 9 can, therefore, be understood from the electrostatic interactions, which are much more significant at pH = 13 once sufficiently arrest occurs. In other words, orientation-dependent particle interactions become negligible at high enough volume fractions that restrict particle rotation, making their interactions equivalent to the spherical particles case. Additionally, a “combined” effect where the particle-particle aggregation is reaction-limited, while the cluster-cluster aggregation at larger length scales is diffusion-limited, is also possible, although proving this is beyond the scope of this work. This will be a topic of a future study.

Once the static experiments were completed both samples were subjected to a series of shear rates and USANS measurements were

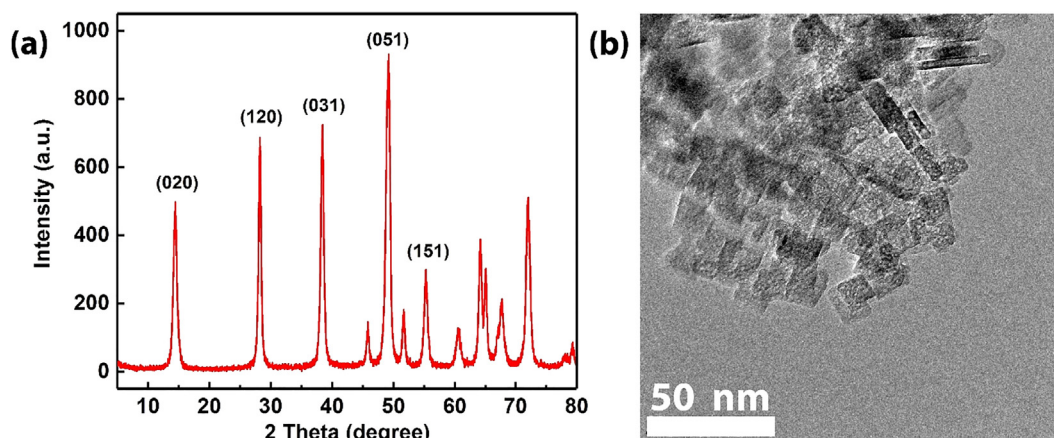


Fig. 1. XRD pattern (a) and TEM image (b) of the as-synthesized boehmite nanocrystals.

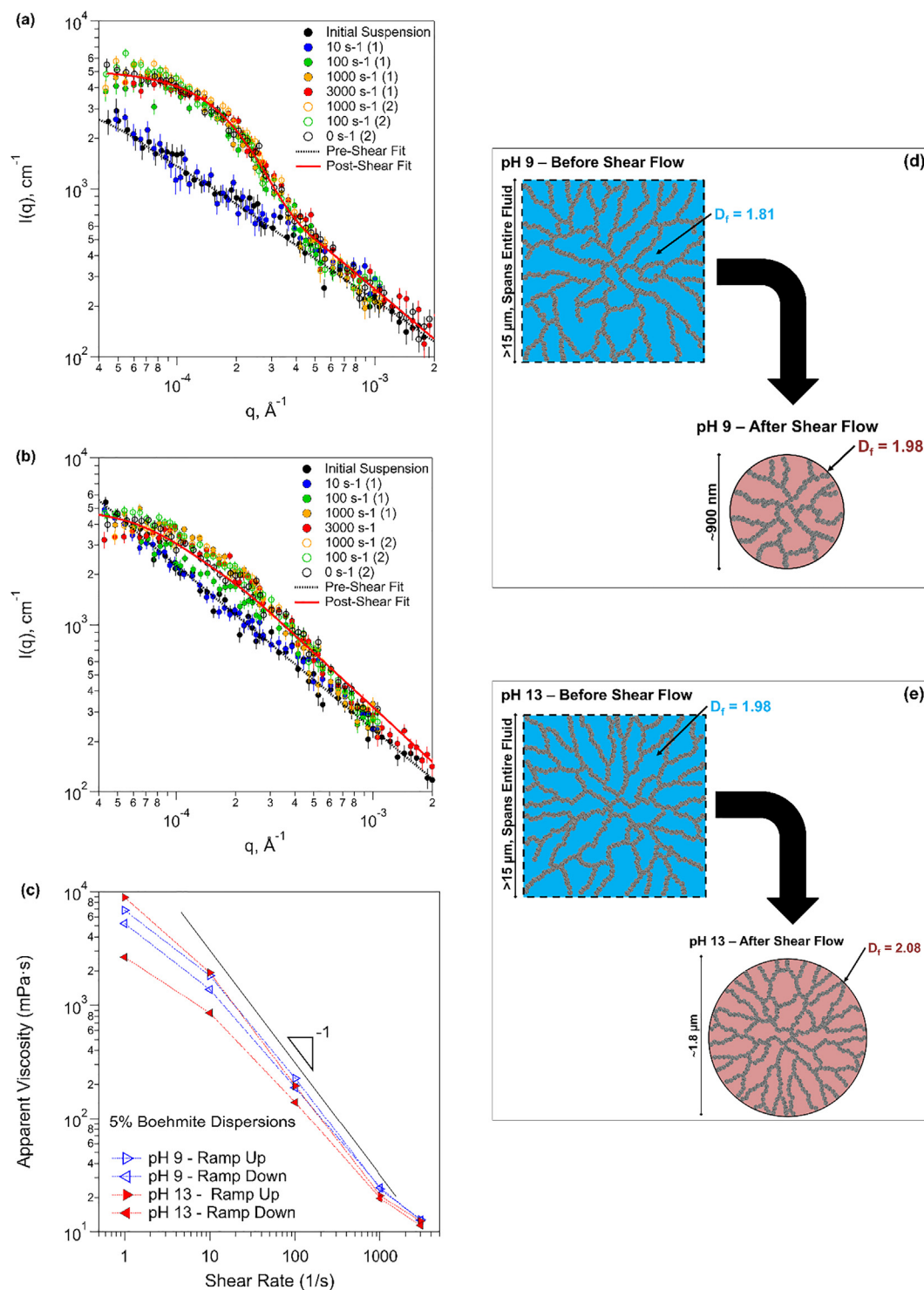


Fig. 2. USANS scattering curves for 5% (w/v) suspensions of boehmite nanocrystals suspended in aqueous solutions at pH 9 (a) and pH 13 (b) at different shear rates. For each sample, the shear rate was first increased and then decreased through the same set of values. Additionally, (c) shows the apparent viscosity as a function of shear rate for the suspensions at the start of each USANS measurement. The data indicate that, at both pHs, the suspensions undergo irreversible changes in agglomerate morphology and rheology. USANS measurements indicate that the boehmite network transitions from a relatively uniform, system-spanning network into a collection of agglomerates of finite size. The unified fit model proposed by Beaucage [ref] was used to fit the radius of gyration and fractal dimension of the particle agglomerates, with the best fits of the pre-shear and post-shear structure shown as solid lines in (a) and (b). The structural changes result in a decrease in the apparent viscosity of the suspensions. Scattering curves are colored according to the shear rate they represent, with upward-pointing triangle symbols for measurements conducted during the increasing shear rate ramp and downward-pointing triangle symbols indicating measurements conducted during the decreasing shear rate ramp. The length-scales and degrees of rearrangement caused by the steady shear are illustrated in (d) and (e). Note: these illustrations are not to scale and are 2-D representations of a 3-D particle network.

made while the sample was being sheared. Scattering curves for these experiments are shown in Fig. 2. For both pH's, the lowest shear rate tested (10 s^{-1}) does not induce any measurable change

in the particle network structure relative to the initial, unsheared sample. The structure does, however, change when both samples are subjected to a shear rate of 100 s^{-1} , indicating that a critical

shear rate (or shear stress) is encountered between 10 and $\sim 100 \text{ s}^{-1}$. The critical shear rate can be qualitatively understood as the minimal shear rate above which hydrodynamic forces overcome the net interparticle attractive force, inducing fragmentation and restructuring of the agglomerates. However, the probability of changing agglomerate morphology by shearing also depends on the agglomerate fractal dimension. That is, it depends on the particle configuration of (i.e., the number of contacts between nearby particles). This is analogous to the physical rationale for yield stress [43].

At elevated shear rates the scattering curves acquire a low q plateau, indicating the presence of fractal agglomerate ‘flocs’ with a finite (measurable) diameter. Fitting these data to the unified radius of gyration model proposed by (solid red lines in Fig. 2(a) and (b)) shows that, after exposure to elevated shear, the structure is composed of finitely sized agglomerates with a fractal dimension slightly larger than that of the unsheared particle network. At pH 9, the fitted fractal dimension is 1.98 ± 0.05 , a significant increase from that of the unsheared sample (1.81 ± 0.04). The agglomerate ‘flocs’ have an average radius of gyration of $890 \pm 20 \text{ nm}$. In the pH 13 sample, post-shear fitting indicated a fractal dimension of 2.09 ± 0.02 (increased from 1.98 ± 0.02 before shearing) and an agglomerate radius of gyration of $1800 \pm 220 \text{ nm}$. This indicates that shear flow causes partial fragmentation, and some densification, of the particle network, the latter to account for the fraction of boehmite particles no longer incorporated in a fractal, fluid-spanning network. The smaller agglomerate flocs at pH 9 indicate that the restructured network, like the initial one, is affected by the interparticle forces. In conjunction with the reaction-limited aggregation pathway indicated by previous studies at low boehmite concentrations, this suggests densification may occur because shear flow provides sufficient force to allow the network to rearrange into a more energetically stable state.

For the pH 9 sample, no further statistically-significant structural changes occur after the initial rearrangement at 100 s^{-1} despite exposing the sample to shear rates in excess of an order of magnitude higher. For the pH 13 sample, some additional restructuring occurs when the shear rate is ramped from 100 s^{-1} to 1000 s^{-1} , but at higher shear rates no further structural rearrangement of the particle network was observed. In general, a larger probability of shear-induced structural changes by is expected for agglomerates with smaller fractal dimensions. Therefore, a higher shear rate would be expected to cause more restructuring in the pH = 9 sample than the pH = 13 sample, the opposite of what was observed. The observed changes also indicate that the critical shear rate (or shear stress) required to cause the particle network to restructure is associated with the length scales probed in USANS. In addition, neither sample shows any significant signs of restructuring after shear flow ceases. Static scattering measurements taken after the shear ramp (black data points connected by a dashed line) are essentially indistinguishable from all other measurements at shear rates $> 1000 \text{ s}^{-1}$, so the final state of the agglomerates appears to be relatively stable.

These results indicate that a sufficiently strong, steady shear can cause irreversible changes to the agglomerate morphology and rheological properties of the boehmite slurries. Due to the consistency of this “before” and “after” state of the structure following exposure to a sufficiently high shear rate (or shear stress), only fits to the static sample before shearing and the static sample after shearing are shown in Fig. 2a and 2b. Attempts to fit and analyze the scattering patterns within each subgroup risk over-interpretation of results due to the intrinsically low signal-to-noise measurement. Therefore, the other scattering data are included primarily for illustrative purposes.

As would be expected, the irreversible structural changes observed by USANS result in irreversible changes to the apparent

viscosity (Fig. 2(c)). There is noticeable change in the flow curves for both samples after exposure to elevated shear rates. However, the magnitude of the change in apparent viscosity is largest at the lowest shear rates. This may reflect the relative importance of non-hydrodynamic forces, such as electrostatic and van der Waals forces, relative to hydrodynamic force (which scale with the shear rate). At lower shear rates, apparent viscosity is expected to be much more dependent on non-hydrodynamic forces, whereas hydrodynamic forces will become increasingly important as the shear rate increases, eventually dictating the apparent viscosity. This has been demonstrated in recent simulations [21,44]. This may also explain the larger change in the apparent viscosity pH 13 sample, relative to the pH 9 sample, as the amount of surface charge on the boehmite particles is much higher at pH 13 than at pH 9, which is near the PZC of boehmite. Thus non-hydrodynamic forces should be stronger at pH13 than at pH9 and more shear should be needed to affect a given change in the structure, although this will also be affected by the differences in the initial fractal dimensions of the particle networks. Disruption of a denser fractal network should result in a larger change in rheological behavior as the number of intercluster ‘bonds’ being broken/disturbed will be much larger, as the number of particles at the edge of a cluster scales with the fractal dimension [45]. Thus the relative behavior of the system at pH 13 is likely the result of stronger electrostatic interactions at short length scales, than at pH 9.

Fig. 2c also shows that both suspensions are highly shear thinning, with a portion of the flow curve having a power-law slope ≈ -1 . This could indicate the presence of shear-banding, but the time-dependence and shear-history-dependence of the suspension rheology and opacity of the suspensions make it very difficult to determine the extent of shear-banding in these samples.

The time-dependencies of the apparent viscosity at each shear rate during the shear rate ramp up are shown in Fig. 3 as normalized apparent viscosity (η/η_0) as a function of time, where η_0 is the initial apparent viscosity for each experiment. Mirroring the USANS measurements discussed previously, there is relatively little change in apparent viscosity below 100 s^{-1} for either sample. At 100 s^{-1} steady shear, however, the apparent viscosity of both samples decreases substantially, dropping 25–30%. Just as in the USANS experiments, the pH 9 sample does not undergo any further substantial changes at higher shear rates, but the apparent viscosity of the pH 13 sample continues to change at 1000 s^{-1} . Again, this is likely due to the differences in the electrostatic forces between the pH = 13 and pH = 9 samples. The restructuring of the pH = 9 sample at 100 s^{-1} leads to a stronger particle network structure, as indicated by the observed increase in fractal dimension. At pH 13, however, the appreciably different electrostatic interactions allow restructuring to continue at higher shear rates due to a relatively weak particle network structure. A small change in relative apparent viscosity is also observed at 3000 cm^{-1} that is not apparent in the pH 9 data, suggesting that some restructuring is occurring in that experiment as well. While no corresponding structural change was observed in the USANS data this may simply reflect the relatively large uncertainties in the USANS measurements.

3.3. Time-dependence of structural and rheological properties under steady shear

A series of further rheological measurements were made to better characterize the effects of the structural rearrangement observed by USANS. A pair of small amplitude oscillatory shear (SAOS) measurements (strain amplitude and frequency sweeps) were conducted at each pH to measure the initial viscoelastic behavior prior to shear flow. The sample was then exposed to a

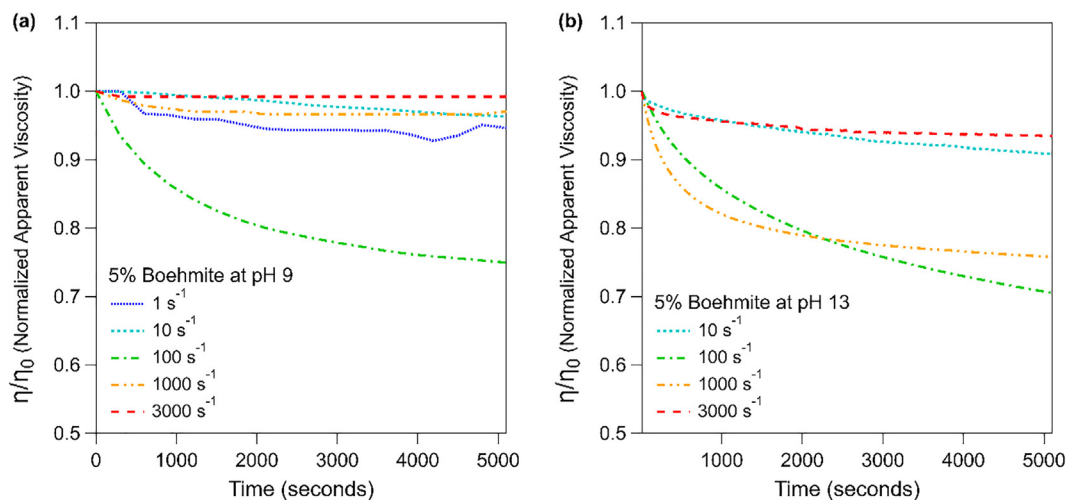


Fig. 3. Plots of normalized apparent viscosity as a function of time for boehmite suspensions at pH 9 (a) and pH 13 (b). The results show that the viscosity is relatively stable below a critical shear rate of $\sim 100 \text{ s}^{-1}$ for both samples. The pH 9 suspension also appears to be relatively stable at higher shear rates. However, at pH 13 the viscosity of the suspension continues to change substantially at 1000 s^{-1} , and observably at 3000 s^{-1} .

period (listed in Fig. 4) of steady shear flow at 100 s^{-1} , the shear rate at which the RheoUSANS results indicated a significant structural change. This was followed by another pair of SAOS measurements. This SAOS/shear/SAOS cycle was then repeated until the sample experienced two hours of cumulative steady shear. As shown in Fig. 4(a), the apparent viscosity of both the pH 9 and pH 13 suspensions decreased when exposed to steady shear, as expected from the RheoSANS measurements (Fig. 3), but increasing the pH affected both the magnitude and dynamics of the restructuring. The apparent viscosity changed more substantially for the pH 13 suspension than the pH 9 suspension and, in addition, the high pH sample was also much more dynamic under quiescent conditions. This can be seen by the recovery in apparent viscosity at the beginning of steady shear following the SAOS measurements (discontinuities in Fig. 4(a & b)). The initial suspensions dynamics are also different. The pH 13 sample experienced a rapid drop in apparent viscosity at the start of the experiment, while the pH 9 sample exhibited a short period of little change followed by a more rapid transition (Fig. 4(b)). This implies that, during quiescence, the interparticle network of the pH 13 sample does not fully recover its original state. Again, this is likely the result from greater electrostatic forces between boehmite particles, and a weaker particle network at pH = 13, leading to dynamic fragmentation/re-aggregation during shearing. This is also consistent with the differences in fractal dimension and probability for structural change discussed above.

The oscillatory measurements provide detailed information about the particle network and further illustrate the substantial effect of solution pH on particle forces. The results of frequency sweep experiments performed at a constant shear strain amplitude of 0.25% are shown in Fig. 4 (c & d). For each frequency sweep the loss factor, $\tan\delta$, is shown as a function of frequency. The loss factor is defined as the ratio of the viscous modulus to the elastic modulus, or G''/G' . Therefore, elastic samples will exhibit a loss factor < 1 and samples with little elasticity will exhibit a loss factor > 1 . Insets in Fig. 4 (c & d) show the complex shear modulus for each measurement (at 5 rad/s). This represents the magnitude of the combined viscous and elastic moduli.

While the loss factors for both samples are almost entirely frequency independent, as expected for particles agglomerated into a fractal network due to no dominant relaxation times, when the samples are exposed to shear, the loss factors for the pH 9 and pH 13 samples respond differently. The pH 9 sample shows a small

decrease in the loss factor (greater elasticity), while the pH 13 sample undergoes a relatively large increase in the loss factor (reduced elasticity), with most of the increase occurring after the first 90 s of steady shear. The complex modulus for the pH 9 sample decreases over the first half hour of steady shear. It then increases slightly over the following 1.5 h, but never recovers the original value. The complex modulus of the pH 13 sample changes substantially after the first exposure to shear, with the complex modulus more than doubling. Following that initial increase, however, the complex modulus of the pH 13 sample decreases with increasing exposure to steady shear.

The strain amplitude sweeps ($\omega = 1 \text{ rad/s}$, Fig. 4e & f) further illustrate the differing effects of shear on the behavior of both suspensions. No substantial change was observed for the pH 9 sample (Fig. 4(e)) beyond a noticeable, monotonic decrease in the shear moduli. The pH 13 sample, however, underwent a much more substantial series of changes. The boundaries of the linear viscoelastic region (the range of strain amplitudes where G' and G'' are independent of strain) are substantially affected by exposure to shear. The critical strain (the strain at which G' and G'' become strain dependent) decreases approximately one order of magnitude over 2 h of steady shear, from $\sim 0.7\%$ to $\sim 0.06\%$. Previous studies [46] have shown that the critical strain for attractive particle suspensions can be related to the length scale of the inter-particle interaction. Here, the shorter interaction lengths could be the result of the increased ionic strength at that pH providing additional screening of electrostatic interactions.

The rheological data thus show that, at pH = 9, steady shear causes no dramatic changes. There is a slight weakening of the particle network (lower G^* and lower $\tan\delta$) and minimal changes in the linear viscoelastic boundary. At pH 13, however, steady shear causes the particle network to initially become stronger, but then weaken. Simultaneously, the network becomes significantly less elastic (increase in $\tan\delta$), and more brittle (very small critical strain/shrinking of the linear viscoelastic region). The more appreciable electrostatic repulsive forces between boehmite particles at pH = 13 (and resultant weaker particle network) are likely responsible for these differences, as the initial particle network is stronger due to the relatively weak electrostatic repulsive forces at pH 9. However, this simple rationale cannot provide detailed explanations for factors such as the opposite trends in the loss factor on shearing and the critical strain decrease for the pH = 13 case. This suggests that coupling to particle shape anisotropy (i.e.,

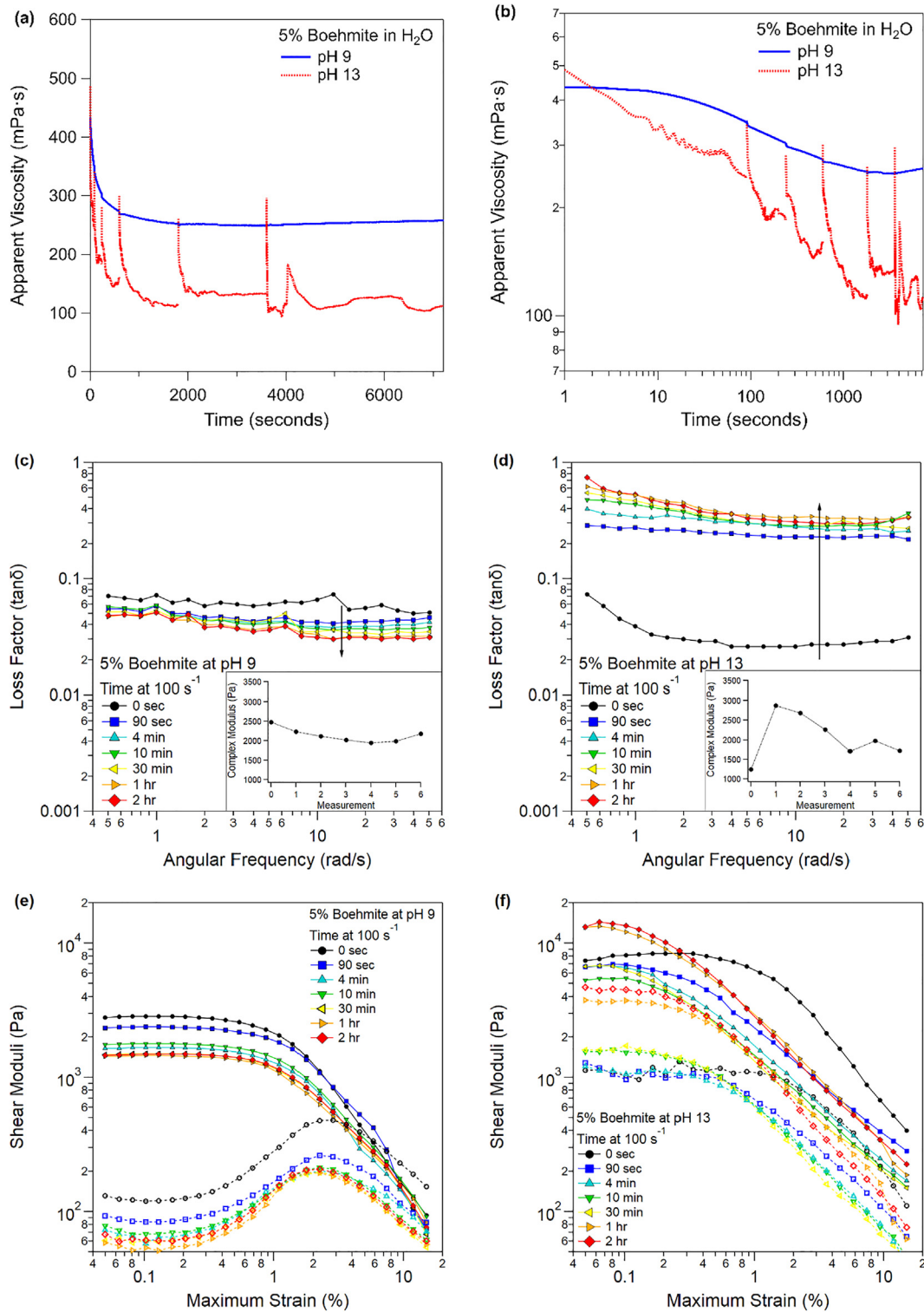


Fig. 4. Experimental results illustrating how exposure to steady shear affects the apparent viscosity, (a-b), and viscoelastic behavior (c-f) of 5% (w/v) suspensions of boehmite at pH 9 (a,c,e) and pH 13 (b,d,f). A sample of the suspension was added to the rheometer and small amplitude oscillatory shear (SAOS) measurements were conducted to measure the initial viscoelasticity. The sample was exposed to a period of steady shear flow at 100 s^{-1} , after which another pair of SAOS measurements were performed. This cycle was continued until the sample experienced two hours of cumulative steady shear. The apparent viscosity decreases for both the pH 9 and pH 13 suspensions when exposed to steady shear (a). In (e) and (f), filled symbols represent the elastic modulus and open symbols represent the viscous modulus for a given sample.

orientation-dependent particle forces) could also be responsible for such complex rheological behavior, although proving this contention is again beyond the scope of this study.

Additional RheoUSANS experiments were used to investigate the structural evolution implied by the rheological changes shown

in Fig. 4. However, because of the low neutron flux available for USANS measurements; a full scan of the scattering vector (q) shown in Fig. 2 can take 12 h to complete, depending on the scattering strength of the sample. Since most of the structural rearrangement occurs in less time than a single USANS scan it is

impossible to probe structural dynamics while the sample is undergoing shear flow. Therefore, the sample was exposed to a constant shear rate for fixed time, the rheometer was stopped, USANS measurement conducted on the static sample, and then the procedure was repeated. These measurements were only carried out using the pH 9 sample, however, because the particle network under quiescent conditions at pH = 13 was insufficiently stability due to the appreciable electrostatic forces between boehmite particles. These are indicated by the large discontinuities in the viscosity vs time curve in Fig. 4(a) for pH13. In contrast, the interparticle network rearrangement during quiescent is rather small at pH9. Although there are small discontinuities upon the start of the next period of steady shear, these are small enough to suggest that this measurement protocol will to capture shear-induced structural changes satisfactorily.

The results of these experiments (Fig. 5) illustrate the structural rearrangement of the particle network occurs under steady shear. During the first 4 min, the power law slope of the scattering curve increases relatively uniformly for $q > \sim 5 \cdot 10^{-4} \text{ \AA}^{-1}$, indicating either formation of very large agglomerate flocs, or densification of the particle network on length scales greater than 1 \mu m . After 10 min, the low q scattering begins to diminish and after 30 min a low- q scattering plateau appears in which scattering intensity is independent of q . This indicates the presence of the same finitely sized agglomerates described previously. After a total of 60 min the scattering curve has acquired the same shape as the final 'equilibrium' structure shown in Fig. 2(a), with a low- q plateau indicating the presence of fractal agglomerate flocs. The sheared sample can, however, recover its original particle network structure if treated using the same sonication procedure used to initially disperse the particles (open symbols in Fig. 5).

3.4. Comparison of Couette and Poiseuille flow

All of the results just described indicate that shear flow significantly affects agglomerate morphology and, thus, the rheology of

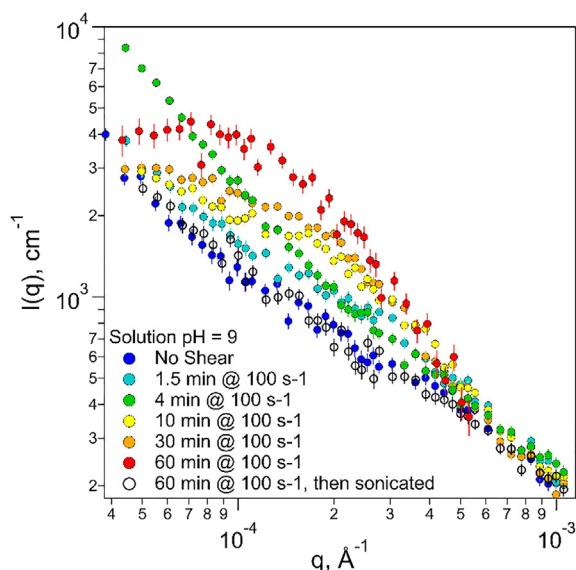


Fig. 5. USANS scattering curves for a 5% (w/v) boehmite dispersion at pH 9 showing how the particle network changes as a function of increasing amounts of time spent flowing at a shear rate of 100 s^{-1} . The sample begins with simple power law scattering profile indicative of a relatively uniform fractal network of particle agglomerates spanning the entire sample. As the sample is exposed to shear flow, the particle network undergoes a structural change, with increasing time a low q plateau appears, indicating the presence of finitely sized agglomerates. Also, the fractal dimension of the particle network increases in the intermediate q region, indicating that the particle network has densified in the corresponding size range.

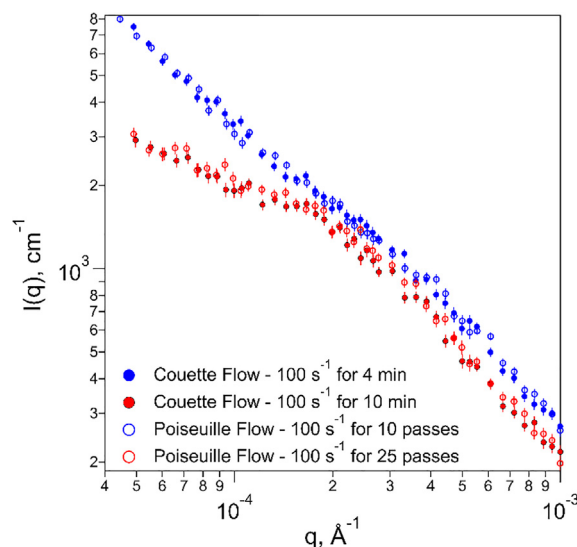


Fig. 6. USANS data showing that exposing the sample to pressure-driven (Poiseuille) flow results in structural changes similar to those generated in Couette flow.

the boehmite suspensions. However, during waste processing, tank samples are very unlikely to encounter a Couette-style shear field. Thus, these results may not be representative of the structural rearrangements that occur in actual waste slurry operations. In fact, prior work has shown that scattering from *in-situ* Couette and Poiseuille flows can be substantially different [47,48]. The model boehmite suspensions were therefore exposed to a pressure-driven pipe flow (Poiseuille flow), as the slurries are much more likely to encounter this type of flow during processing. In these experiments the sample was pushed multiple times through a short length of capillary tubing between two syringes. This design was adopted because shear is not homogeneous across the capillary, but most of the flow is expected to be laminar. Thus, a multiple-pass, short tube system maximizes the chance of exposing most of the sample to high-shear environment near the wall. The number of passes through the tubing was scaled so that the average sample volume experienced the wall shear rate for a time roughly equivalent to the sample in the Couette cell (which has an almost entirely uniform shear rate throughout). Because of these assumptions, however, the data presented Fig. 6 for pressure-driven flow cannot be said to represent exactly equivalent conditions to those in Figures (2–5).

The results of these USANS measurements are shown in Fig. 6, along with scattering curves from Fig. 5 with shear rates and shear strains similar to those of the capillary flow samples. The results suggest that pressure-driven and couette flow cause very similar structural changes to the boehmite particle network.

4. Conclusions

4.1. Key findings

After being dispersed in aqueous solution, boehmite nanocrystals form gels that can undergo relatively drastic structural and rheological changes when subjected to steady shear flow. The particles are initially arranged as a uniform fractal network that spans the entire fluid, with the fractal dimension depending on the electrostatic forces between the boehmite particles. The fractal geometry of the agglomerate structure is also concentration-dependent, as shown by comparing these results to the work of Nakouzi et al. [26]. Exposing the particle suspension to shear flow causes the net-

work to rearrange into a dispersion of finitely-sized agglomerate 'flocs' on the μm size scale. The fractal dimension of the agglomerate particle network also densifies marginally relative to the original gel. These dynamic structural changes can be understood as a balance between kinetically-arrested cluster-cluster aggregation at large length scales and particle-particle aggregation resulting from interparticle forces associated with the particles' surface chemistry and anisotropic shape. The complicated rheological characteristics observed also suggest that the orientation-dependent particle forces observed in previous work do not manifest themselves in the same way at higher solid fractions, where an arrested diffusion-limited aggregation becomes more important. These results are relatively novel in the realm of attractive, colloidal fractal networks, especially considering the irregular/non-spherical shape of the particles. There is a great deal of literature studying reversible time-dependent rheology (thixotropy) in particle suspensions [49–58] with well-developed theoretical models [46,59–64] to help describe the behavior. Irreversible shear-induced structural changes in colloidal systems, however, have been less extensively studied on a fundamental, physical level [65–71]. In fact, many of these studies involve reactive systems (like concrete) where the structural changes are primarily the result of chemical reactions rather than being shear-induced. By contrast, the boehmite suspensions studied here exhibit an extremely complex rheological and structural response to shear flow and may provide a unique model system for probing the behavior of complex suspensions under flow conditions, especially since this complex behavior occurs in a relatively simple suspension of a single particle species and the amount of shear energy required to cause structural rearrangement is readily accessible experimentally.

4.2. Future work

Work is currently underway to more fully understand how the volume fraction of the particles affects aggregation. Preliminary results at a lower solids fraction (2.5 wt% rather than 5 wt%) show that agglomerate fractal dimensions mimic the reaction vs. diffusion aggregation behavior of the very low concentration samples tested previously [26]. Further work is also needed to better understand the kinetics of the shear-induced structural and rheological changes observed. Experiments probing the shear-strain-dependence of these changes could provide further insight into the nature of the phenomena and deconvolute the effects of shear rate, shear stress, and shear strain. Measurement limitations of the Ultra-Small Angle Neutron Scattering technique make it difficult to effectively probe dynamics on the time scales of interest in these suspensions, so experiments using a higher flux X-ray scattering technique are underway. Previous simulation work [26] investigated the rotational diffusion timescale of the particles and agglomerates. Further calculations will investigate the relationship between rotational timescales and 'critical' shear rates for network reorganization. As it is also possible that a certain amount of stress is required for the particle network to rearrange from a local energy minimum to a more stable conformation, this should be investigated simultaneously. Finally, as briefly mentioned, the actual nuclear waste slurry in the tanks at Hanford and Savannah River is much more complex than the system used in this study. Typically it contains an caustic ($\text{pH} > 10$) aqueous solution with high concentrations ($> \sim 0.1 \text{ M}$) of various dissolved salts (e.g., Cs, Cr, Na), an appreciable concentration ($> 5\text{--}10 \text{ wt\%}$) of non-spherical, polydisperse Al and Fe metal oxide/hydroxide particles [72]. Boehmite has been identified as a particularly problematic phase in the waste slurry, as its plate-like shape, sharp-edges, and nanometer-sized of crystals may strongly influence rheology [72]. As shown here, such physicochemical parameters may be

expected to be strongly correlated with the rheological behavior of the waste slurry [73]. Therefore, the model system considered here provides an important starting point for studying the effects of a range of complex physicochemical parameters (e.g., ionic strength, cation and anion charge and size) on the properties of these important waste slurries.

CRedit authorship contribution statement

J.S. Weston: Conceptualization, Methodology, Formal analysis, Investigation, Writing - original draft, Writing - review & editing, Visualization. **J. Chun:** Writing - original draft, Investigation, Formal analysis, Writing - review & editing, Project administration, Funding acquisition. **G. Schenter:** Writing - review & editing, Investigation. **K. Weigandt:** Supervision, Methodology, Formal analysis, Data curation, Conceptualization. **M. Zong:** Writing - review & editing. **X. Zhang:** Resources. **K.M. Rosso:** Writing - review & editing. **L.M. Anovitz:** Writing - review & editing, Investigation, Methodology, Project administration.

Declaration of Competing Interest

The authors declare that they have no known competing financial interests or personal relationships that could have appeared to influence the work reported in this paper.

Acknowledgements

This work was supported by the U.S. Department of Energy (DOE), U.S. National Science Foundation (NSF), and European Union's Horizon 2020 research and innovation program. DOE supported the design of the experiments, theoretical interpretation, and data analysis via IDREAM (Interfacial Dynamics in Radioactive Environments and Materials). This work benefited from the use of the SasView application, originally developed under NSF award DMR-0520547. SasView contains code developed with funding from the European Union's Horizon 2020 research and innovation programme under the SINE2020 project, grant agreement No 654000. A portion of this research was performed using EMSL, a national scientific user facility sponsored by the DOE Office of Biological and Environmental Research and located at Pacific Northwest National Laboratory (PNNL). Access to the BT-5 Ultra-Small Angle Neutron Scattering instrument was provided by the Center for High Resolution Neutron Scattering, a partnership between the National Institute of Standards and Technology and the National Science Foundation under Agreement No. DMR-1508249. PNNL is a multiprogram national laboratory operated for DOE by Battelle Memorial Institute under Contract No. DE-AC05-76RLO-1830.

Appendix A. Supplementary material

Supplementary data to this article can be found online at <https://doi.org/10.1016/j.jcis.2020.03.109>.

References

- [1] H. Van Olphen, *An introduction to Clay Colloid Chemistry: For Clay Technologists, Geologists, and Soil Scientists*, Wiley, 1977. https://books.google.com/books/about/An_Introduction_to_Clay_Colloid_Chemistr.html?id=RLMRAQAAIAJ (accessed June 13, 2019).
- [2] R. Buscall, P.D.A. Mills, R.F. Stewart, D. Sutton, L.R. White, G.E. Yates, The rheology of strongly-flocculated suspensions, *J. Nonnewton. Fluid Mech.* 24 (1987) 183–202. [https://doi.org/10.1016/0377-0257\(87\)85009-7](https://doi.org/10.1016/0377-0257(87)85009-7).
- [3] F. Pignon, A. Magnin, J.-M. Piau, B. Cabane, P. Lindner, O. Diat, Yield stress thixotropic clay suspension: Investigations of structure by light, neutron, and

- x-ray scattering, *Phys. Rev. E* 56 (1997) 3281–3289, <https://doi.org/10.1103/PhysRevE.56.3281>.
- [4] Wierenga, Anieke, A.P. Philipse, H.N.W. Lekkerkerker, D.V. Boger, Aqueous Dispersions of Colloidal Boehmite: Structure, Dynamics, and Yield Stress of Rod Gels, 1998, <https://doi.org/10.1021/LA970376Z>.
- [5] B. Klein, S.J. Partridge, J.S. Laskowski, Rheology of unstable mineral suspensions, *Coal Prep.* 8 (1990) 123–134, <https://doi.org/10.1080/07349349008905180>.
- [6] G.C. Bushell, Y.D. Yan, D. Woodfield, J. Raper, R. Amal, On techniques for the measurement of the mass fractal dimension of aggregates, *Adv. Colloid Interface Sci.* 95 (2002) 1–50, [https://doi.org/10.1016/S0001-8686\(00\)00078-6](https://doi.org/10.1016/S0001-8686(00)00078-6).
- [7] P. Snabre, P. Mills, Rheology of weakly flocculated suspensions of rigid particles, *J. Phys. III* (6) (1996) 1811–1834, <https://doi.org/10.1051/jp3:1996215>.
- [8] E. Lattuada, S. Buzzaccaro, R. Piazza, Compressive yield stress of depletion gels from stationary centrifugation profiles 044005, *J. Phys. Condens. Matter* 30 (2018), <https://doi.org/10.1088/1361-648X/aaa2d1>.
- [9] J. Vermant, M.J. Solomon, Flow-induced structure in colloidal suspensions, *J. Phys. Condens. Matter* 17 (2005) R187–R216, <https://doi.org/10.1088/0953-8984/17/4/R02>.
- [10] G.R. Zeichner, W.R. Schowalter, Effects of hydrodynamic and colloidal forces on the coagulation of dispersions, *J. Colloid Interface Sci.* 71 (1979) 237–253, [https://doi.org/10.1016/0021-9797\(79\)90235-2](https://doi.org/10.1016/0021-9797(79)90235-2).
- [11] J.V. DeGroot, C.W. Macosko, T. Kume, T. Hashimoto, Flow-induced anisotropic SALS in silica-filled PDMS liquids, *J. Colloid Interface Sci.* 166 (1994) 404–413, <https://doi.org/10.1006/JCIS.1994.1311>.
- [12] S.R. Raghavan, S.A. Khan, Shear-induced microstructural changes in flocculated suspensions of fumed silica, *J. Rheol. (N. Y. N. Y.)* 39 (1995) 1311–1325, <https://doi.org/10.1122/1.550638>.
- [13] P. Rehinder, Coagulation and thixotropic structures, *Discuss. Faraday Soc.* 18 (1954) 151, <https://doi.org/10.1039/d9541800151>.
- [14] Z. Varga, J.W. Swan, Large scale anisotropies in sheared colloidal gels, *J. Rheol. (N. Y. N. Y.)* 62 (2018) 405–418, <https://doi.org/10.1122/1.5003364>.
- [15] DOE, Secretary of Energy Advisory Board Report of the Task Force on Technology Development for Environmental Management, 2014. https://www.energy.gov/sites/prod/files/2015/01/f19/Report_of_the_SEAB_Task_Force_on_Tech_Development_for_EM_FINAL.pdf (accessed January 27, 2019).
- [16] M.H. Nielsen, D. Li, H. Zhang, S. Aloni, T.Y.-J. Han, C. Frandsen, J. Seto, J.F. Banfield, H. Cölfen, J.J. De Yoreo, Investigating processes of nanocrystal formation and transformation via liquid cell TEM, *Microsc. Microanal.* 20 (2014) 425–436, <https://doi.org/10.1017/S1431927614000294>.
- [17] J.J. De Yoreo, P.U.P.A. Gilbert, N.A.J.M. Sommerdijk, R.L. Penn, S. Whitlam, D. Joester, H. Zhang, J.D. Rimer, A. Navrotsky, J.F. Banfield, A.F. Wallace, F.M. Michel, F.C. Meldrum, H. Cölfen, P.M. Dove, Crystallization by particle attachment in synthetic, biogenic, and geologic environments, *Science* (80-). 349 (2015) aaa6760–aaa6760, <https://doi.org/10.1126/science.aaa6760>.
- [18] T.J. Woehl, J.E. Evans, I. Arslan, W.D. Ristenpart, N.D. Browning, Direct in situ determination of the mechanisms controlling nanoparticle nucleation and growth, *ACS Nano* 6 (2012) 8599–8610, <https://doi.org/10.1021/nn303371y>.
- [19] T.J. Woehl, C. Park, J.E. Evans, I. Arslan, W.D. Ristenpart, N.D. Browning, Direct observation of aggregative nanoparticle growth: kinetic modeling of the size distribution and growth rate, *Nano Lett.* 14 (2014) 373–378, <https://doi.org/10.1021/nl4043328>.
- [20] H. Zheng, R.K. Smith, Y.-W. Jun, C. Kisielowski, U. Dahmen, A.P. Alivisatos, Observation of single colloidal platinum nanocrystal growth trajectories, *Science* 324 (2009) 1309–1312, <https://doi.org/10.1126/science.1172104>.
- [21] S. Pednekar, J. Chun, J.F. Morris, Simulation of shear thickening in attractive colloidal suspensions, *Soft Matter* 13 (2017) 1773–1779, <https://doi.org/10.1039/C6SM02553F>.
- [22] S. Pednekar, J. Chun, J.F. Morris, Bidisperse and polydisperse suspension rheology at large solid fraction, *J. Rheol. (N. Y. N. Y.)* 62 (2018) 513–526, <https://doi.org/10.1122/1.5011353>.
- [23] A. Can Zaman, C.B. Üstünda, A. Kara, F. Kaya, C. Kaya, Carbon nanotube/boehmite-derived alumina ceramics obtained by hydrothermal synthesis and spark plasma sintering (SPS), *J. Eur. Ceram. Soc.* 30 (2010) 3351–3356, <https://doi.org/10.1016/j.jeurceramsoc.2010.07.037>.
- [24] R. Tettenhorst, D.A. Hofmann, Crystal chemistry of boehmite, *Clays Clay Miner.* 28 (1980) 373–380, <https://doi.org/10.1346/CCMN.1980.0280507>.
- [25] L.M. Anovitz, X. Zhang, J. Soltis, E. Nakouzi, A.J. Krzysko, J. Chun, G.K. Schenter, T.R. Graham, K.M. Rosso, J.J. De Yoreo, A.G. Stack, M. Bleuel, C. Gagnon, D.F.R. Mildner, J. Ilavsky, I. Kuzmenko, Effects of ionic strength, salt, and pH on aggregation of boehmite nanocrystals: tumbler small-angle neutron and X-ray scattering and imaging analysis, *Langmuir* 34 (2018) 15839–15853, <https://doi.org/10.1021/acs.langmuir.8b00865>.
- [26] E. Nakouzi, J.A. Soltis, B.A. Legg, G.K. Schenter, X. Zhang, T.R. Graham, K.M. Rosso, L.M. Anovitz, J.J. De Yoreo, J. Chun, Impact of solution chemistry and particle anisotropy on the collective dynamics of oriented aggregation, *ACS Nano* 12 (2018) 10114–10122, <https://doi.org/10.1021/acsnano.8b04909>.
- [27] X. Zhang, W. Cui, K.L. Page, C.L. Pearce, M.E. Bowden, T.R. Graham, Z. Shen, P. Li, Z. Wang, S. Kerisit, A.T. N'Diaye, S.B. Clark, K.M. Rosso, Size and morphology controlled synthesis of boehmite nanoplates and crystal growth mechanisms, *Cryst. Growth Des.* 18 (2018) 3596–3606, <https://doi.org/10.1021/acs.cgd.8b00394>.
- [28] J.G. Barker, C.J. Glinka, J.J. Moyer, M.H. Kim, A.R. Drews, M. Agamalian, Design and performance of a thermal-neutron double-crystal diffractometer for USANS at NIST, *J. Appl. Crystallogr.* 38 (2005) 1004–1011, <https://doi.org/10.1107/S0021889805032103>.
- [29] A. Mohraz, D.B. Moler, R.M. Ziff, M.J. Solomon, Effect of monomer geometry on the fractal structure of colloidal rod aggregates 155503, *Phys. Rev. Lett.* 92 (2004), <https://doi.org/10.1103/PhysRevLett.92.155503>.
- [30] S.R. Kline, Reduction and analysis of SANS and USANS data using IGOR Pro, *J. Appl. Crystallogr.* 39 (2006) 895–900, <https://doi.org/10.1107/S0021889806035059>.
- [31] G. Beaucage, Small-angle scattering from polymeric mass fractals of arbitrary mass-fractal dimension, *J. Appl. Crystallogr.* 29 (1996) 134–146, <https://doi.org/10.1107/S0021889895011605>.
- [32] B. Hammouda, Analysis of the Beaucage model, *J. Appl. Crystallogr.* 43 (2010) 1474–1478, <https://doi.org/10.1107/S0021889810033856>.
- [33] J. Weston, S. Hudson, K. Weigandt, Probing the structure of high viscosity complex fluids at extreme shear rates, in: *Eng. Sci. Fundam. 2017 - Core Program. Area 2017 AIChE Annu. Meet.*, 2017.
- [34] R. Wessel, R.C. Ball, Fractal aggregates and gels in shear flow, *Phys. Rev. A* 46 (1992) R3008–R3011, <https://doi.org/10.1103/PhysRevA.46.R3008>.
- [35] M.E. Helgeson, Y. Gao, S.E. Moran, J. Lee, M. Godfrin, A. Tripathi, A. Bose, P.S. Doyle, Homogeneous percolation versus arrested phase separation in attractively-driven nanoemulsion colloidal gels, *Soft Matter* 10 (2014), <https://doi.org/10.1039/c3sm52951g>.
- [36] V. Grenard, T. Divoux, N. Taberlet, S. Manneville, Timescales in creep and yielding of attractive gels, *Soft Matter* 10 (2014) 1555, <https://doi.org/10.1039/c3sm52548a>.
- [37] H.M. Wyss, E.V. Tervoort, L.J. Gauckler, Mechanics and microstructures of concentrated particle gels, *J. Am. Ceram. Soc.* 88 (2005) 2337–2348, <https://doi.org/10.1111/j.1551-2916.2005.00622.x>.
- [38] A. Pek-Ing, L. Yee-Kwong, Surface chemistry and rheology of Laponite dispersions – Zeta potential, yield stress, ageing, fractal dimension and pyrophosphate, *Appl. Clay Sci.* 107 (2015) 36–45, <https://doi.org/10.1016/j.clay.2015.01.033>.
- [39] J.S. Weston, D. Venkataramani, C.P. Aichele, B.P. Grady, J. Harwell, D. Resasco, Pseudosolid, shear-thinning gel formation in binary dispersions of metal oxide nanoparticles at low volume fractions, *Langmuir* 30 (2014), <https://doi.org/10.1021/la503442a>.
- [40] M.Y. Lin, H.M. Lindsay, D.A. Weitz, R. Klein, R.C. Ball, P. Meakin, Universal diffusion-limited colloid aggregation, *J. Phys. Condens. Matter* 2 (1990) 3093–3113, <https://doi.org/10.1088/0953-8984/2/13/019>.
- [41] M.Y. Lin, H.M. Lindsay, D.A. Weitz, R.C. Ball, R. Klein, P. Meakin, Universality in colloid aggregation, *Nature* 339 (1989) 360–362, <https://doi.org/10.1038/339360a0>.
- [42] G.A. Parks, The isoelectric points of solid oxides, solid hydroxides, and aqueous hydroxo complex systems, *Chem. Rev.* 65 (1965) 177–198, <https://doi.org/10.1021/cr60234a002>.
- [43] W.B. Russel, D.A. Saville, W.R. Schowalter, *Colloidal dispersions*, Cambridge University Press, 1989. https://books.google.com/books/about/Colloidal_Dispersions.html?id=80W5QgAACAAJ (accessed September 13, 2019).
- [44] A. Singh, S. Pednekar, J. Chun, M.M. Denn, J.F. Morris, From Yielding to Shear Jamming in a Cohesive Frictional Suspension 098004, *Phys. Rev. Lett.* 122 (2019), <https://doi.org/10.1103/PhysRevLett.122.098004>.
- [45] B.B. Mandelbrot, *Les objets fractals : forme, hasard et dimension*, Flammarion, 1975.
- [46] J. Mewis, N.J. Wagner, *Colloidal suspension rheology*, Cambridge University Press (2011), <https://doi.org/10.1017/CBO9780511977978>.
- [47] V.M. Cloke, J.S. Higgins, C.L. Phoon, S.M. Richardson, S.M. King, R. Done, T.E. Cooper, Poiseuille geometry shear flow apparatus for small-angle scattering experiments, *Rev. Sci. Instrum.* 67 (1996) 3158–3163, <https://doi.org/10.1063/1.1147439>.
- [48] J.S.J.S. Weston, D.P.D.P. Seeman, D.L.D.L. Blair, P.F.P.F. Salipante, S.D.S.D. Hudson, K.M.K.M. Weigandt, Simultaneous slit rheometry and in situ neutron scattering, *Rheol. Acta* 57 (2018) 241–250, <https://doi.org/10.1007/s00397-018-1073-0>.
- [49] P. Coussot, A.I. Leonov, J.M. Piau, Rheology of concentrated dispersed systems in a low molecular weight matrix, *J. Nonnewton. Fluid Mech.* 46 (1993) 179–217, [https://doi.org/10.1016/0377-0257\(93\)85046-D](https://doi.org/10.1016/0377-0257(93)85046-D).
- [50] A. Potanin, Thixotropy and rheology of aggregated dispersions with wetting polymer, *J. Rheol. (N. Y. N. Y.)* 48 (2004) 1279–1293, <https://doi.org/10.1122/1.1807844>.
- [51] B.D. Marsh, Viscoelastic hysteresis. Part II. Numerical and experimental examples, *Trans. Soc. Rheol.* 12 (1968) 489–510, <https://doi.org/10.1122/1.549093>.
- [52] W. Wolthers, M.H.G. Duits, D. van den Ende, J. Mellema, Shear history dependence of the viscosity of aggregated colloidal dispersions, *J. Rheol. (N. Y. N. Y.)* 40 (1996) 799–811, <https://doi.org/10.1122/1.550783>.
- [53] H.A. Mercer, H.D. Weymann, Structure of thixotropic suspensions in shear flow – 3. Time-dependent behavior, *Trans. Soc. Rheol.* 18 (1974) 199–218, <https://doi.org/10.1122/1.549356>.
- [54] R.C. Sonntag, W.B. Russel, Structure and breakup of flocs subjected to fluid stresses. I. Shear experiments, *J. Colloid Interface Sci.* 113 (1986) 399–413, [https://doi.org/10.1016/0021-9797\(86\)90175-X](https://doi.org/10.1016/0021-9797(86)90175-X).

- [55] K. Dullaert, J.J. Mewis, A model system for thixotropy studies, *Rheol. Acta* 45 (2005) 23–32, <https://doi.org/10.1007/s00397-005-0439-2>.
- [56] M.I. Aranguren, E. Mora, C.W. MacOsco, Compounding fumed silicas into polydimethylsiloxane: Bound rubber and final aggregate size, *J. Colloid Interface Sci.* 195 (1997) 329–337, <https://doi.org/10.1006/jcis.1997.5143>.
- [57] R. Mendes, G. Vinay, G. Ovarlez, P. Coussot, Reversible and irreversible destructuring flow in waxy oils: An MRI study, *J. Nonnewton. Fluid Mech.* 220 (2015) 77–86, <https://doi.org/10.1016/j.jnnfm.2014.09.011>.
- [58] C.O. Osuji, C. Kim, D.A. Weitz, Shear thickening and scaling of the elastic modulus in a fractal colloidal system with attractive interactions, *Phys. Rev. E - Stat. Nonlinear, Soft Matter Phys.* 77 (2008), <https://doi.org/10.1103/PhysRevE.77.060402>.
- [59] Z. Kemblowski, J. Petera, A generalized rheological model of thixotropic materials, *Rheol. Acta.* 19 (1980) 529–538, <https://doi.org/10.1007/BF01517508>.
- [60] D. Doraiswamy, A.N. Mujumdar, I. Tsao, A.N. Beris, S.C. Danforth, A.B. Metzner, The Cox-Merz rule extended: A rheological model for concentrated suspensions and other materials with a yield stress, *J. Rheol. (N. Y. N. Y.)* 35 (1991) 647–685, <https://doi.org/10.1122/1.550184>.
- [61] R.B. Bird, B.D. Marsh, Viscoelastic hysteresis. Part I. Model predictions, *Trans. Soc. Rheol.* 12 (1968) 479–488, <https://doi.org/10.1122/1.549096>.
- [62] R. Buscall, P.D.A. Mills, J.W. Goodwin, D.W. Lawson, Scaling behaviour of the rheology of aggregate networks formed from colloidal particles, *J. Chem. Soc. Faraday Trans. 1 Phys. Chem. Condens. Phases* 84 (1988) 4249–4260, <https://doi.org/10.1039/F19888404249>.
- [63] N.P. Thien, R.I. Tanner, A new constitutive equation derived from network theory, *J. Nonnewton. Fluid Mech.* 2 (1977) 353–365, [https://doi.org/10.1016/0377-0257\(77\)80021-9](https://doi.org/10.1016/0377-0257(77)80021-9).
- [64] H.A. Barnes, Thixotropy - A review, *J. Nonnewton. Fluid Mech.* 70 (1997) 1–33, [https://doi.org/10.1016/S0377-0257\(97\)00004-9](https://doi.org/10.1016/S0377-0257(97)00004-9).
- [65] L. Starrs, W.C.K. Poon, D.J. Hibberd, M.M. Robins, Collapse of transient gels in colloid-polymer mixtures, *J. Phys. Condens. Matter.* 14 (2002) 2485–2505, <https://doi.org/10.1088/0953-8984/14/10/302>.
- [66] J.V. Degroot, C.W. Macosko, Aging phenomena in silica-filled polydimethylsiloxane, *J. Colloid Interface Sci.* 217 (1999) 86–93, <https://doi.org/10.1006/jcis.1999.6332>.
- [67] E.C. Rodrigues, P.R. de Souza Mendes, Predicting the time-dependent irreversible rheological behavior of oil well cement slurries, *J. Pet. Sci. Eng.* 178 (2019) 805–813, <https://doi.org/10.1016/j.petrol.2019.03.073>.
- [68] D.E.V. Andrade, P. Coussot, Brittle solid collapse to simple liquid for a waxy suspension, *Soft Matter* 15 (2019) 8766–8777, <https://doi.org/10.1039/c9sm01517e>.
- [69] F.H. Marchesini, R.M. Oliveira, H. Althoff, P.R. de Souza Mendes, Irreversible time-dependent rheological behavior of cement slurries: Constitutive model and experiments, *J. Rheol. (N. Y. N. Y.)* 63 (2019) 247–262, <https://doi.org/10.1122/1.5054879>.
- [70] S.C. Schulz, J. Schlutter, S.T. Buschhorn, K. Schulte, W. Bauhofer, Rheological properties and irreversible dispersion changes in carbon nanotube/epoxy systems, *Polym. Eng. Sci.* 52 (2012) 849–855, <https://doi.org/10.1002/pen.22151>.
- [71] H.J.M. Hanley, C.D. Muzny, B.D. Butler, G.C. Straty, J. Bartlett, E. Drabarek, Shear-induced restructuring of concentrated colloidal silica gels, *J. Phys. Condens. Matter.* 11 (1999) 1369–1380, <https://doi.org/10.1088/0953-8984/11/6/003>.
- [72] R.A. Peterson, E.C. Buck, J. Chun, R.C. Daniel, D.L. Herting, E.S. Ilton, G.J. Lumetta, S.B. Clark, Review of the scientific understanding of radioactive waste at the U.S. DOE Hanford site, *Environ. Sci. Technol.* 52 (2018) 381–396, <https://doi.org/10.1021/acs.est.7b04077>.
- [73] J. Chun, T. Oh, M. Luna, M. Schweiger, Effect of particle size distribution on slurry rheology: Nuclear waste simulant slurries, *Colloids Surf. A Physicochem. Eng. Asp.* 384 (2011) 304–310, <https://doi.org/10.1016/j.colsurfa.2011.04.003>.